Superlattices and Microstructures 146 (2020) 106650

Contents lists available at ScienceDirect

Superlattices and Microstructures

journal homepage: www.elsevier.com/locate/superlattices

DFT investigation of H_2S adsorption on graphenenanosheets and nanoribbons: Comparative study

Ehab Salih [a], Ahmad I. Ayesh [a,b,*]

[a] Department of Mathematics, Statistics and Physics, Qatar University, P. O. Box 2713, Doha, Qatar
[b] Center for Sustainable Development, Qatar University, P. O. Box 2713, Doha, Qatar

ARTICLE INFO

Keywords:
Graphene
Zigzag
Armchair
Nanoribbons
H_2S adsorption
Gas sensor

ABSTRACT

Graphenenanosheet (GNS), armchair graphenenanoribbon (AGNR), and zigzag graphenenanoribbon (ZGNR) systems were investigated by first principle calculations using the density functional theory (DFT). The DFT calculations explored the potential of utilization of these materials as gas sensors to detect hydrogen sulfide (H_2S) gas. H_2S gas adsorption was explored using: the adsorption energy (E_{ads}), adsorption distance (D), charge transfer (ΔQ), density of states (DOS), and band structure of the generated systems before and after adsorption of H_2S. The results showed that E_{ads} of bare ZGNR was the highest of −0.171 eV as compared with GNS and AGNR. The surfaces of GNS, AGNR, and ZGNR have been modified with epoxy and then with a hydroxyl groups. The adsorption capacity of the three systems has been enhanced after the modifications with both the epoxy and hydroxyl groups. Based on the adsorption energy and charge transfer results, hydroxyl modified ZGNR system can be used effectively for detection applications of H_2S since it exhibits the highest charge transfer and large adsorption energy.

1. Introduction

Emission of toxic gases from industrial applications represents an environmental hazard and serious threat to all creatures on the earth. A considerably hazardous gas is hydrogen sulfide (H_2S) that is mainly produced from petroleum extraction, natural gas, and decomposition of organic matter [1]. The safe threshold concentration for H_2S gas is set to 20 parts per million (ppm) for 8 h work load as stated by the Occupational Safety and Health Administration (OSHA) [2]. The dangerous effects of H_2S on human health extends from irritation of eyes at low concentrations to loss of consciousness and possible death in case of exposure to high concentrations [3–5]. Consequently, the concentration of H_2S gas in air should be detected rapidly, accurately, and conveniently [6,7]. The gas detectors are normally characterized by their sensitivity, selectivity, and response time which are critical parameters to choose the suitable of sensing system [8].

A significant trend of research has been established recently on using materials that exhibit at least one of their dimensions in the range from 1 to 100 nm (nanomaterials) to build highly sensitive and low cost sensors [7,9]. Nanomaterials (NMs) are considered as optimum systems for the applications that include gas adsorption because of their high surface area to volume ratio and hollow structure [9]. From the various categories of NMs, carbon based nanomaterials (C-NMs), have gained a considerable interest in the last couple of decades thanks to their remarkable electronic, magnetic, and optical properties, as well as their chemical versatility and biocompatibility [10–13]. Different studies have been published recently on using C-NMs in the field of gas sensors. For instance,

* Corresponding author. Department of Mathematics, Statistics and Physics, Qatar University, P. O. Box 2713, Doha, Qatar.
E-mail address: ayesh@qu.edu.qa (A.I. Ayesh).

https://doi.org/10.1016/j.spmi.2020.106650
Received 29 June 2020; Accepted 7 July 2020
Available online 15 July 2020

pristine and functionalized zigzag carbon nanotubes (CNT) were used to detect the toxic H_2S gas [9]. Particularly, they have studied the adsorption of H_2S on pristine CNT and its Boron/Nitrogen functionalized forms and found that the sensitivity and recovery time of pristine CNT were better than its Boron and Nitrogen functionalized forms [9]. Another study has reported the detection of H_2S gas based on amido-functionalized single-walled carbon nanotube (SWCNT) [14]. On the other hand, doped fullerenes have been also studied as a gas sensor to detect the toxic H_2S gas [15]. In this study, the adsorptive capability was enhanced upon doping fullerenes with various dopants including N, S, B, P, and Si through providing additional negative adsorption energy. The researchers have finally found that the strongest interaction energy was detected for the case of B-doped fullerenes. In addition, many articles have been published recently on using C-NMs to detect the toxic H_2S gas [16–18].

Among these C-NMs, graphene has been extensively studied recently for the field of gas sensors because of its outstanding mechanical properties as well as electrical and thermal conductivities. Graphene is described as a two dimensional material with a single atom thickness, and was firstly produced experimentally in 2004 [19–21]. Each carbon atom in graphene forms three σ bonds in graphene's plane with sp^2 hybridization and the other perpendicular p_z orbital makes π covalent bond [22–24]. In spite of its remarkable properties, graphene has some limitations in the field of sensors due to its zero band gap nature [25]. This issue can be handled either by modifying the surface of graphene by functional groups such as epoxy and hydroxyl groups, or fabricating graphene structure that exhibits a band gap, i.e. graphene nanoribbons (GNR) [25,26]. Based on edge termination and arrangements of carbon atoms, GNR can be classified into zigzag graphenenaEnoribbons (ZGNR) and armchair graphenenanoribbons (AGNR) [27,28]. As a result of localization of the wave function at their edges, ZGNR behaves like a metal while AGNR behaves like a semiconductor due to quantum confinement and edge states [24,27].

In addition to fabrication and characterization of graphene based NMs using different experimental techniques, its remarkable properties as well as the promising applications have been also widely studied theoretically [29]. Moreover, the modification of graphene was found to be a reason for enhancing the electrical conductivity, electrolyte wettability, capacitance, and electrode accessibility [30,31]. For example, the detection of H_2S was studied based on pure and doped graphene [32]. In this study, the authors compared between the adsorption parameters of pure graphene and boron, aluminum, and gallium doped graphene. The results demonstrated an improvement in the adsorption energy as well as the adsorption distance upon doping graphene with aluminum, and gallium. Pristine and Pt-decorated graphene sheets have been used in another study as gas sensor to detect the toxic H_2S gas [33]. The results of this paper showed that decorating graphene with Pt improved significantly the adsorption parameters as compared with pristine graphene thanks to chemisorption of the toxic H_2S gas molecule [33]. Moreover, different articles have been published in the recent years that investigate the surface modification of graphene and GNR with different functional groups, for example as epoxy and hydroxyl groups, and its utilization to detect different gases [6,34–40].

In this work, different from the previously mentioned articles, we compared between the sensing performance of three different graphene based materials (GNS, AGNR, and ZGNR) to detect the toxic H_2S gas. The GNS, AGNR, and ZGNR systems were built using Atomistic ToolKit Virtual NanoLab (ATK-VNL) based on the generalized gradient approximations (GGA). Moreover, the sensing performance of the GNS, AGNR, and ZGNR systems was enhanced upon introducing epoxy and hydroxyl groups to their surfaces.

2. Computational method

Adsorption of H_2S gas on the surface of GNS, AGNR, and ZGNR systems was studied by DFT calculations using ATK-VNL package (version 2018.06). The generalized gradient approximation (GGA) with the Perdew-Burke-Ernzerhof (PBE) exchange correlation was selected as the processing method [41,42]. An unpolarized basis set, a density mesh cutoff of 125 Hartree, and force tolerance of 0.01 eV/Å were chosen during the calculations for all systems. In all calculations of GNS, a Monkhorst–Pack k point sampling of $4 \times 4 \times 1$ was used, while k-point sampling of $4 \times 2 \times 1$ was used for AGNR and ZGNR. The changes in the adsorption energy (E_{ads}), charge transfer (ΔQ), adsorption distance (D) (i.e. the shortest direct distance between the gas molecule and the system), band structure, and density of states (DOS) have been investigated to confirm the adsorption of H_2S gas on the surfaces of GNS, AGNR, and ZGNR systems. The adsorption energy of each system: GNS, AGNR, and ZGNR to H_2S gas molecule was calculated by the following formula [36,43–45]:

$$\boldsymbol{E}_{ads} = \boldsymbol{E}_{G+functional\ group+gas} - (\boldsymbol{E}_{G+functional\ group} + \boldsymbol{E}_{gas})$$

where $E_{G+functional\ group+gas}$ is the total energy of either GNS, AGNR, or ZGNR system after the adsorption of H_2S gas on its surface. $E_{G+functional\ group}$ is the total energy of either GNS, AGNR, or ZGNR systems (including the functional group, if any), and E_{gas} is the total energy of the optimized H_2S gas. The more negative value of E_{ads} reflects a configuration with enhanced stability as well as stronger adsorption of H_2S gas [46,47]. Moreover, the charge transfer of H_2S gas has been calculated based on the Mulliken population using the following formula [48,49]:

$$\Delta Q = Q_a - Q_b$$

where Q_a and Q_b are the Mulliken charges of the gas after and before the adsorption, respectively.

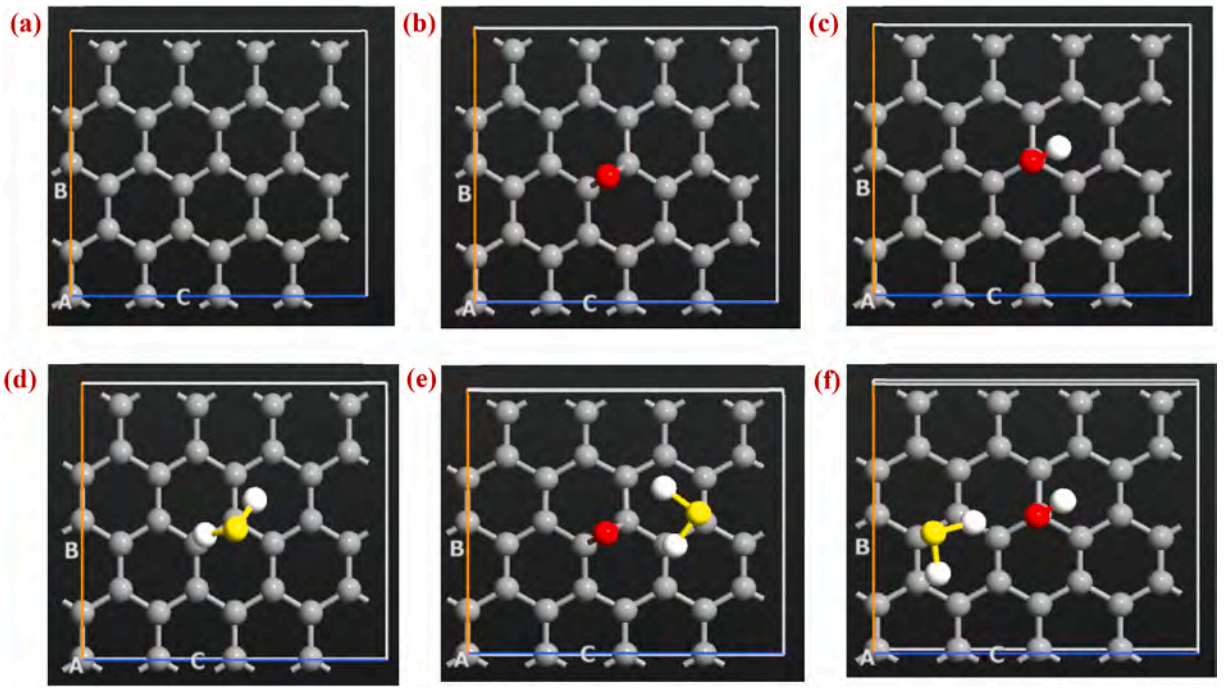

Fig. 1. Top view of the optimized a) GNS, b) GNS-O, c) GNS-OH, d) GNS-H_2S, e) GNS-*O*-H_2S, and f) GNS–OH–H_2S.

Table 1
Adsorption energy (E_{ads}), adsorption distance (D), band gap and charge transfer (ΔQ) of GNS, AGNR and ZGNR systems after the adsorption of H_2S gas.

System	E_{ads}(eV)	D (Å)	Band gap (eV)	ΔQ (e)
GNS-H_2S	−0.149	3.32	0.000	−0.015
GNS-*O*-H_2S	−0.190	3.12	0.283	−0.033
GNS–OH–H_2S	−0.249	3.05	0.000	−0.093
AGNR-H_2S	−0.101	3.50	0.838	−0.022
AGNR-*O*-H_2S	−0.204	2.66	0.942	−0.027
AGNR–OH–H_2S	−0.261	2.77	0.000	−0.061
ZGNR-H_2S	−0.171	3.29	0.000	−0.014
ZGNR-*O*-H_2S	−0.194	3.12	0.000	−0.019
ZGNR–OH–H_2S	−0.252	2.22	0.088	−0.097

3. Results and discussion

3.1. Graphene nanosheets

Bare GNS is used without modification to detect H_2S gas as a first stage. To improve the adsorption capacity, the surface is then modified with oxygen to form GNS-O system and hydroxyl group to form GNS-OH system. The optimized structures of GNS, GNS-O, and GNS-OH before and after the adsorption of H_2S gas are shown in Fig. 1. The C–C bond length is 1.43 Å, the C–O bond in case of GNS-O is 1.46 Å, and the C–O and O–H bonds in case of GNS-OH are 1.5 Å and 0.98 Å, respectively. The C–C bond length around the epoxy and hydroxyl groups increase to 1.5 Å after the modification. The adsorption energies, adsorption distance, band gap, and charge transfer of the three systems after H_2S adsorption are given in Table 1. The adsorption capacity of GNS towards H_2S is found to be enhanced by modifying the GNS with the epoxy and the hydroxyl groups. However, the best performance is for the case of GNS-OH with adsorption energy of −0.245 eV and charge transfer of −0.093 e. Fig. 2 shows the band structures of GNS, GNS-O, and GNS-OH systems before and after adsorption of H_2S. The band structure results reveal that GNS (Fig. 2a) has a zero band gap due to the overlapping between the valence and conduction bands which is in good agreement with the literatures [50,51]. Although, no dramatic changes are detected in the band gap due to modification with epoxy and the hydroxyl groups, some modifications appear below and above the Fermi level confirming the adsorption of H_2S gas. In the case of GNS-O (Fig. 2b), the band gap has increased to 0.292 eV due to the existence of oxygen. This band gap decrease in the case of GNS-*O*-H_2S (Fig. 2e) to 0.283 eV which confirms the adsorption of H_2S. A new band appears at the Fermi level in the cases of GNS-OH and GNS–OH–H_2S (Fig. 2c and f), giving it a zero band gap due to the presence of the hydroxyl group. Fig. 3 shows the density of states of the three systems before and after gas adsorption. The density

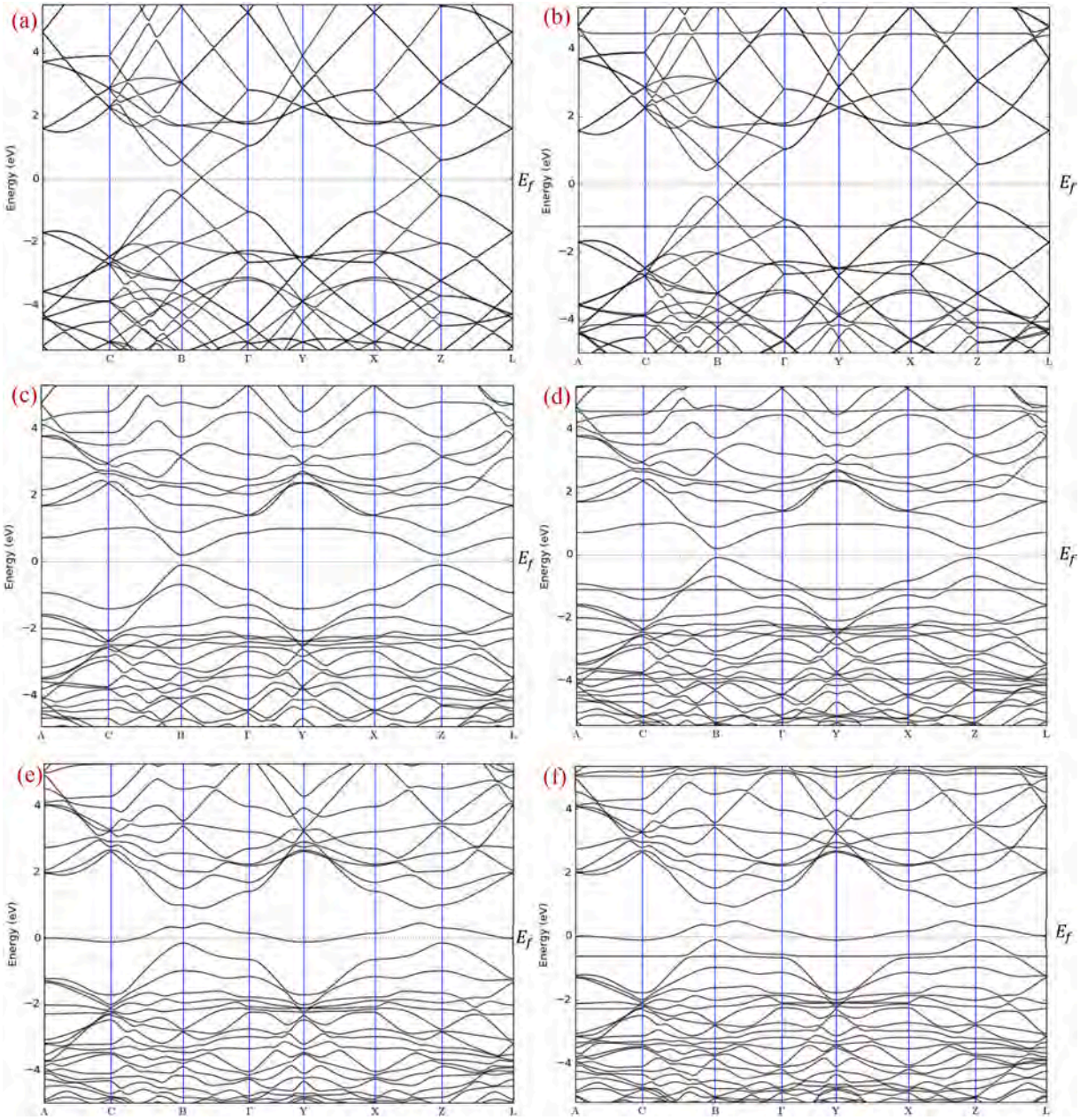

Fig. 2. Band Structure of a) GNS, b) GNS-H_2S, c) GNS-O, d) GNS-*O*-H_2S, e) GNS-OH, and f) GNS–OH–H_2S.

of states at the Fermi level is zero for the cases of GNS and GNS-O and about 3 $(eV)^{-1}$ for the case of GNS-OH, which confirms the band structure results. Although no significant changes can be observed at the Fermi level, there is a considerable increase in the density of the sates at around −13.0, −6.0, −1.4, 5.5, 8.0, and 13.0 eV for the case of GNS (Fig. 3a) confirming the adsorption of H_2S gas. In the case of GNS-O (Fig. 3b), three small peaks appear around −23.0, 22.5, and 23.5 eV due to the presence of the oxygen. Besides, a considerable increase in the intensity of the peak at around 23.5 eV is detected which proves that the epoxy group is involved in adsorption of H_2S. Additional peak around −21.0 eV is observed in the case of GNS-OH (Fig. 3c) because of the hydroxyl group.

3.2. Armchair graphene nanoribbons

In this part, the adsorption of H_2S gas on AGNR, AGNR-O, and AGNR-OH systems is investigated. Fig. 4 shows the optimized structures of AGNR, AGNR-O, and AGNR-OH systems before and after H_2S adsorption. In case of AGNR, the C–C bond length is 1.43 Å, while at the edges the C–C bond length decreases to 1.24 Å due to the edge reconstruction that occur at the edges of bare GNR which is

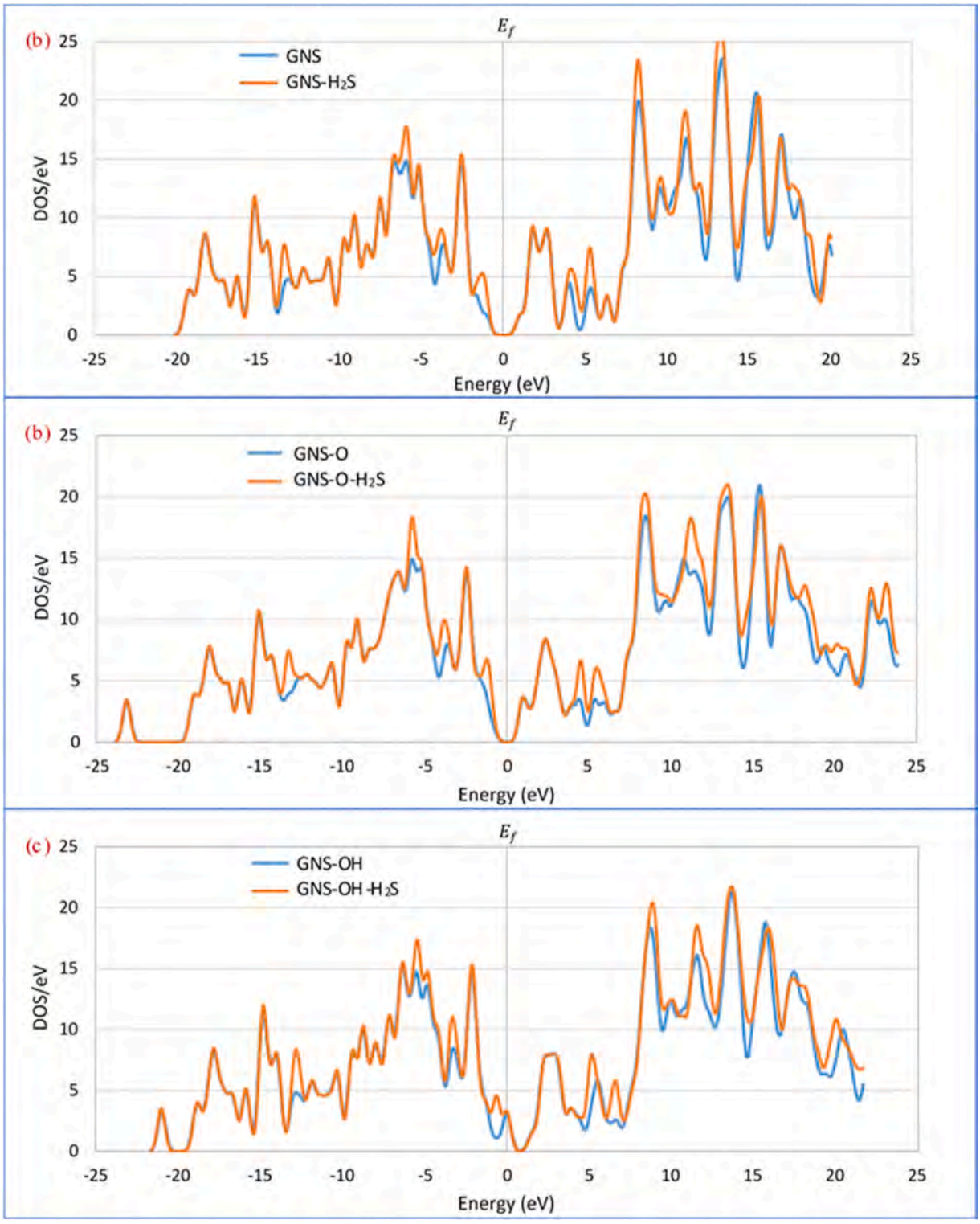

Fig. 3. Density of states of a) GNS and GNS-H_2S, b) GNS-O and GNS-*O*-H_2S, and c) GNS-OH and GNS–OH–H_2S.

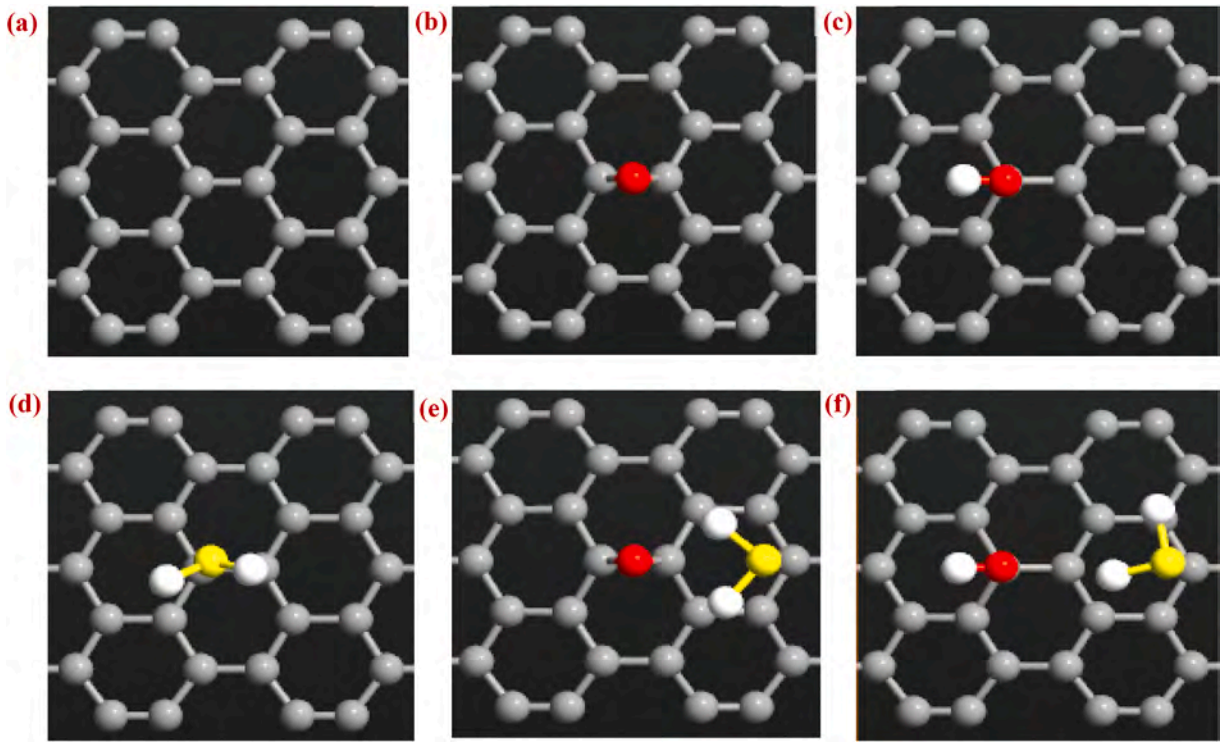

Fig. 4. Top view of the optimized a) AGNR, b) AGNR-O, c) AGNR-OH, d) AGNR-H_2S, e) AGNR-*O*-H_2S, and f) AGNR–OH–H_2S.

in agreement with some of the reported values [52,53]. Meanwhile, the C–O bond for AGNR-O is 1.47 Å. The C–O and O–H bonds in the case of AGNR-OH are 1.47 Å and 0.98 Å, respectively. The C–C bond length around epoxy and hydroxyl groups increase a little to 1.5 Å after the modification. The adsorption energies, adsorption distance, band gap, and charge transfer of the three systems after H_2S adsorption are given in Table 1. Before modifying AGNR with epoxy and hydroxyl groups, the adsorption energy, adsorption distance, and charge transfer are found to be −0.101 eV, 3.50 Å, and −0.022 e, respectively. On the other hand, the adsorption energy is almost doubled for the case of AGNR-O and become −0.261 eV in the case of AGNR-OH. Moreover, the charge transfer increases to −0.027 and −0.061 e for AGNR-O and AGNR-OH, respectively, reflecting that addition of epoxy and hydroxyl groups on the surface of AGNR plays a vital role to improve the adsorption capacity of AGNR towards H_2S gas. The band structure of the three systems before and after gas adsorption are investigated and the results are presented in Fig. 5. The band structure results show that AGNR system (Fig. 5a) has a 0.844 eV band gap before the adsorption of H_2S reflecting its semiconductor nature. This value decreases slightly after gas adsorption to 0.838 eV. For the case of AGNR-O, the band gap increases to 0.945 eV due to the presence of oxygen. This value then decreases to 0.942 eV after the adsorption of H_2S gas. Because of the hydroxyl group, the band gap value of AGNR-OH is zero for both cases: before and after the adsorption. No significant changes are observed for the band gap before and after the adsorption, while some changes appear below and above the Fermi level confirming the adsorption of H_2S. Fig. 6 shows the density of states of the three systems before and after the adsorption of H_2S gas. On one hand, no remarkable changes are observed at the Fermi level before and after the adsorption, but a small peak appears for the case of AGNR-OH confirming the zero band gap obtained by the band structure studies (Fig. 5e and f). On the other hand, the density of states around −13.0, −6.0, −4.0, 5.0, 10.6, 13.5, 18.0, and 19.7 eV increase significantly after H_2S adsorption on AGNR. The same behavior is observed for the cases of AGNR-O and AGNR-OH confirming the successful adsorption of H_2S. Moreover, some new peaks appear at −22.0, 9.0 and 22.7 eV for the case of AGNR-O and −21.0, 9.0, and 22.3 eV for the case of AGNR-OH due to the presence of the epoxy and hydroxyl groups. The considerable changes in the density of states that appear at 22.7 eV for the case of AGNR-O and 22.3 eV for the case of AGNR-OH reflect the contribution of the oxygen and hydroxyl on the adsorption process of H_2S.

3.3. Zigzag graphene nanoribbons

The effects of H_2S adsorption on ZGNR, ZGNR-O, and ZGNR-OH systems are studied in this part. Fig. 7 shows the optimized structures of ZGNR, ZGNR-O, and ZGNR-OH systems before and after H_2S adsorption. For the case of ZGNR, the C–C bond length is 1.44 Å, while at the edges, the C–C bond length decreases slightly to 1.41 and 1.39 Å as a result of the edge reconstruction. Moreover, the C–O and O–H bonds for the case of ZGNR-OH are 1.49 Å and 0.98 Å, respectively. The C–C bond length around the hydroxyl group increases slightly to 1.5 Å after the modification. For the case of ZGNR-O, the C–O bond length is 1.39 Å. ZGNR is first used to detect H_2S gas and it shows −0.171 eV and −0.014 e, respectively, adsorption energy and charge transfer as indicated in Table 1. A significant

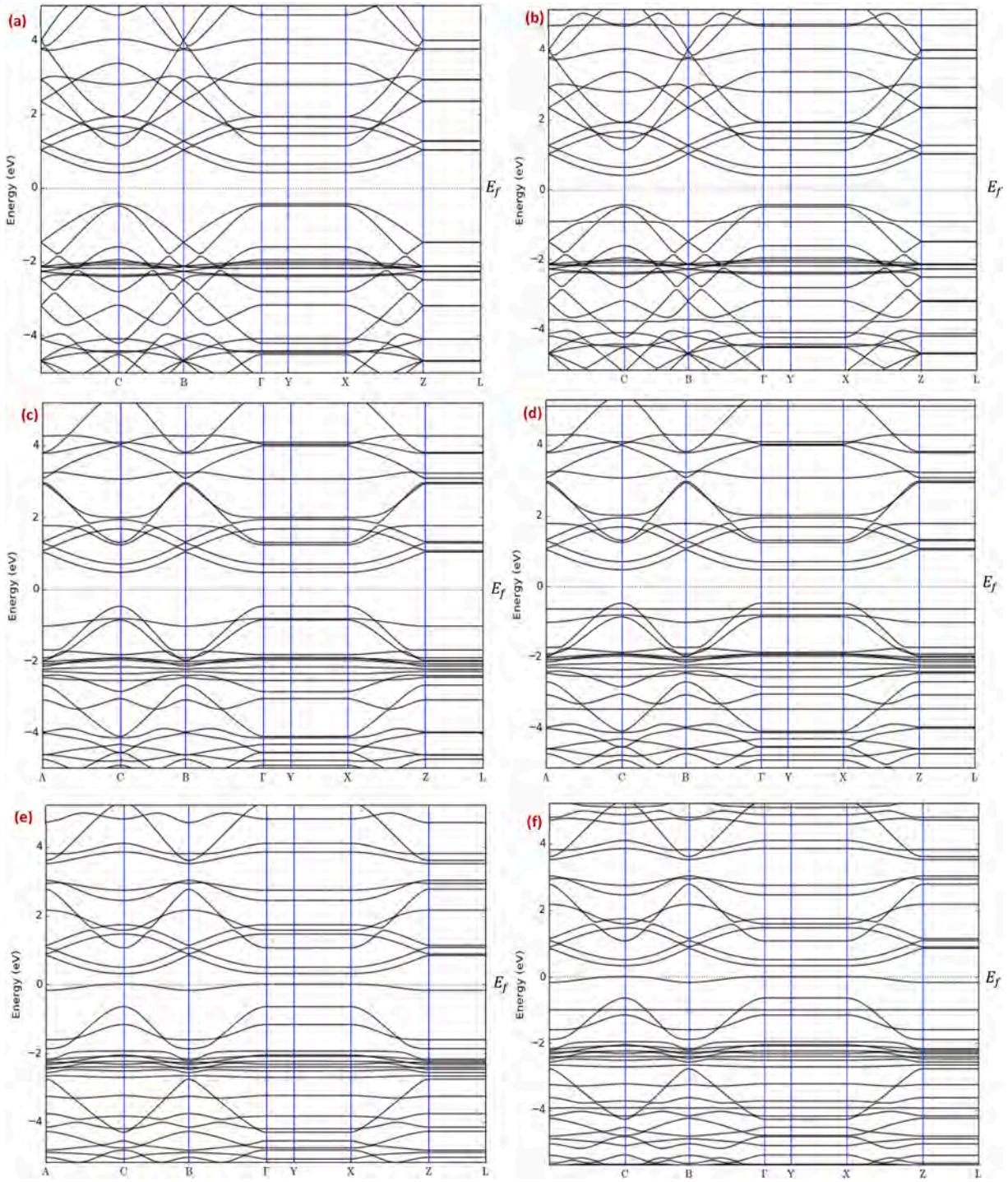

Fig. 5. Band Structure of a) AGNR, b) AGNR-H_2S, c) AGNR-O, d) AGNR-*O*-H_2S, e) AGNR-OH, and f) AGNR–OH–H_2S.

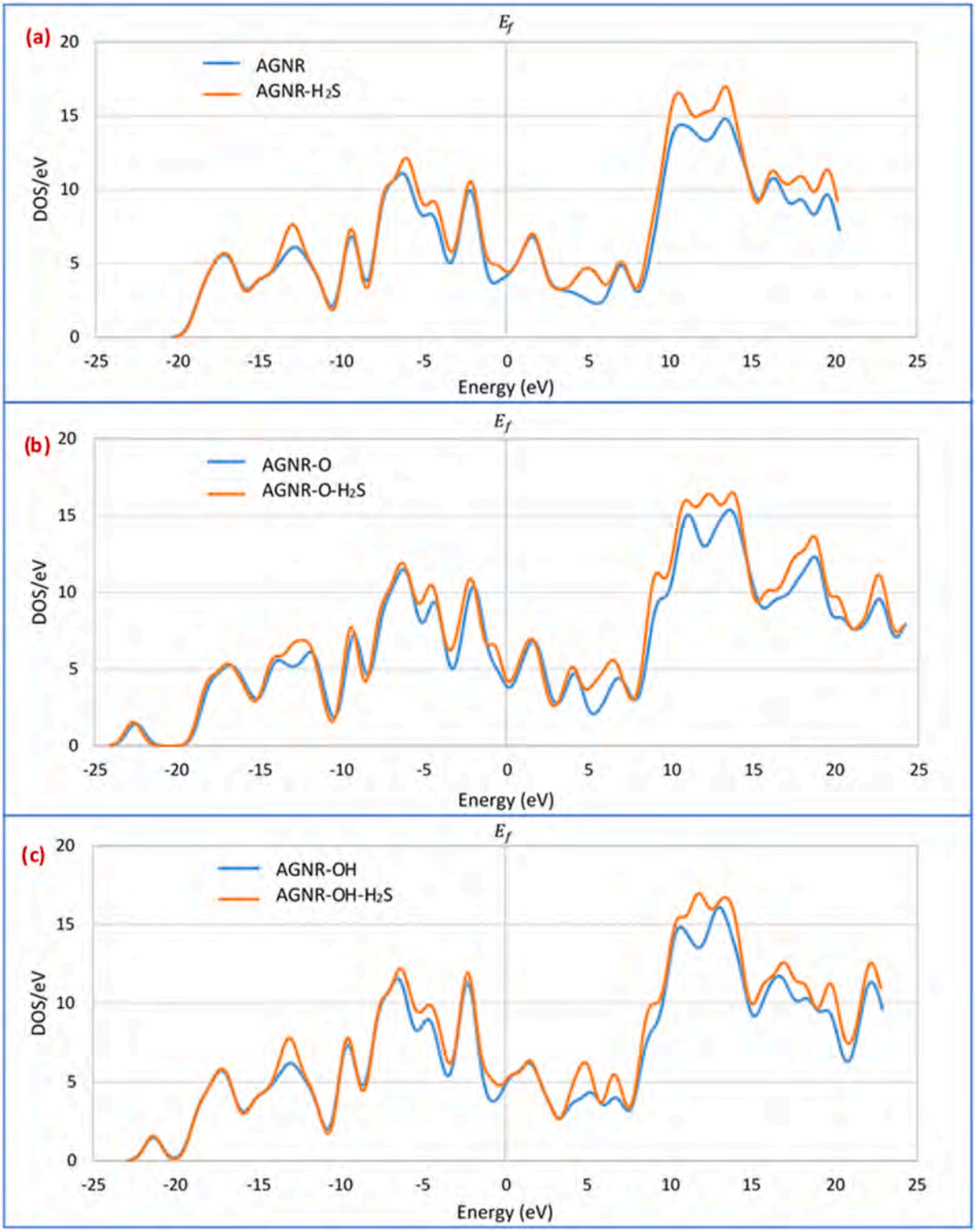

Fig. 6. Density of states of a) AGNR and AGNR-H_2S, b) AGNR-O and AGNR-*O*-H_2S, and c) AGNR-OH and AGNR–OH–H_2S.

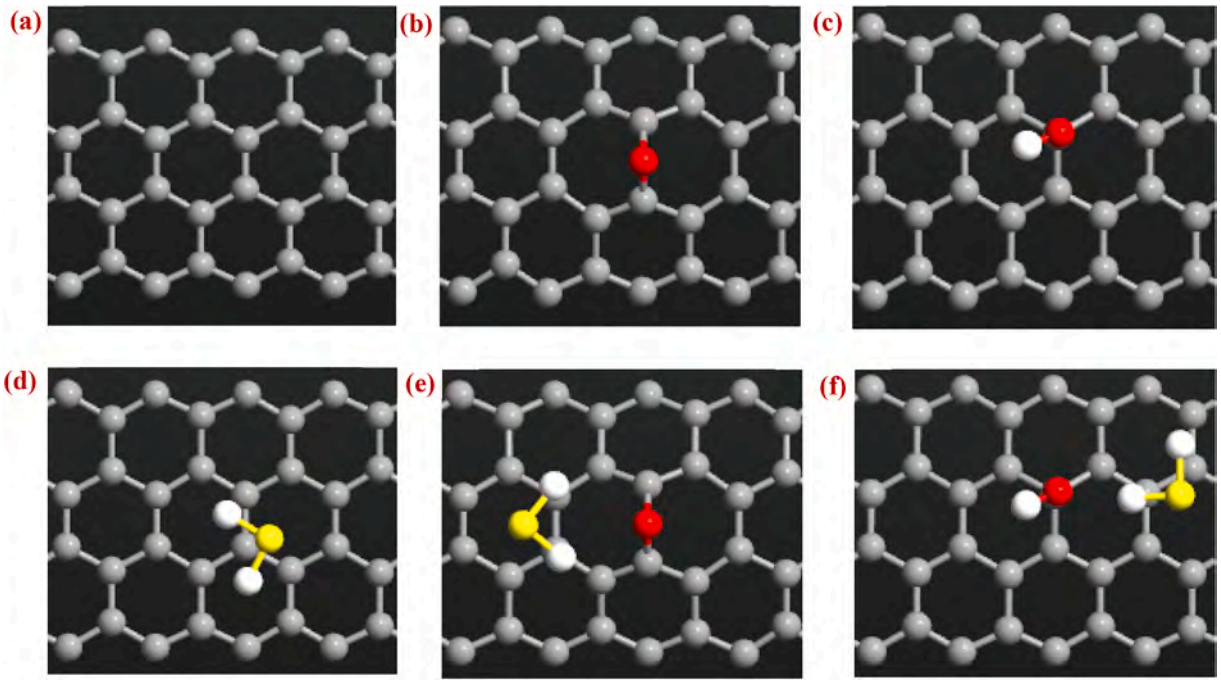

Fig. 7. Top view of the optimized a) ZGNR, b) ZGNR-O, c) ZGNR-OH, d) ZGNR-H_2S, e) ZGNR-*O*-H_2S, and f) ZGNR–OH–H_2S.

improvement in the adsorption capacity is noticed after surface modification of ZGNR with epoxy and hydroxyl groups. The case of ZGNR–OH–H_2S exhibits the highest adsorption energy and charge transfer with values of −0.252 eV and −0.097 e, respectively.

The band gap analysis conform the metallic nature of ZGNR, where the band gap is zero before and after H_2S adsorption for the three systems except for the case of ZGNR–OH–H_2S with 0.088 eV as shown in Fig. 8. No remarkable changes are found in the band structures before and after adsorption of H_2S on ZGNR, ZGNR-O, and ZGNR-OH systems. In contrast, the three systems reveal conductivity improvement as a result of H_2S adsorption as demonstrated by the density of states results (Figs. 9(a)-9(c)).

As shown for the case of ZGNR in Fig. 9a, the density of states at the Fermi level increases slightly as a result of modifying the conductivity of ZGNR after adsorption of H_2S. Moreover, a remarkable increase in the density of states around −5.0, −3.0, 4.9, 10.2, and 19.4 eV are observed after H_2S gas adsorption. Fig. 9b indicates the appearance of new peaks around −23.0, 20.3, and 22.3 eV for the case of ZGNR-O. The new peaks may be attributed to the formation of the epoxy group. After H_2S gas adsorption, the two peaks at 20.3 and 22.3 eV combine and a new peak result at 21.5 eV indicating the contribution of the epoxy group for the process of H_2S detection. After modification of ZGNR with the hydroxyl group, two new peaks around −21.0 and 21.8 eV are detected as shown in Fig. 9c. The density of states at −21.0 eV is almost fixed before and after the adsorption process. However, a significant increase at 21.8 eV is observed reflecting the contribution of the hydroxyl group on the adsorption of H_2S gas.

3.4. Comparison between the three systems

In this part, a comparison between the performance of GNS, AGNR, and ZGNR systems before and after modification as sensors to detect H_2S gas in terms of adsorption distance, adsorption energy, and charge transfer is presented. Fig. 10a reveals a comparison between the adsorption distances of all systems. Before modification, the smallest adsorption distance was found in the case of ZGNR with 3.29 Å. After modification, the adsorption distance decreases for the three systems. The smallest adsorption distance between H_2S gas and the systems is for the case of ZGNR-OH with 2.22 Å. Fig. 10b shows that the adsorption energy is the highest with a value of −0.171 eV for the case of ZGNR before modification. After modification, the adsorption energy increases significantly for the three systems with both epoxy or hydroxyl groups. The highest adsorption energy is for the case of AGNR-OH with −0.261 eV which is almost similar value for ZGNR-OH with −0.252 eV, nevertheless, ZGNR-OH exhibits the highest charge transfer. Fig. 10c demonstrates a comparison between the values of charge transfer for all systems. The highest charge transfer before modification is for the case of pure AGNR with −0.022 e. After modification, the charge transfer increases remarkably especially for the case of hydroxyl modification with a value of −0.097 e for the case of ZGNR-OH. Comparing the adsorption distance, adsorption energies, and charge transfer results, the hydroxyl modified ZGNR system exhibits almost the highest adsorption capacity which is consistent with the highest charge transfer and low adsorption distance. Therefore, the results suggest that the ZGNR-OH is the best system in this study to be considered as a potential gas sensor for H_2S.

Intrinsic graphene face main challenges that hinder its application for the field of sensors including the difficulty of its production on large scale, absence of any functional groups on its surface, and the absence of any band gap (which leads to metal-like

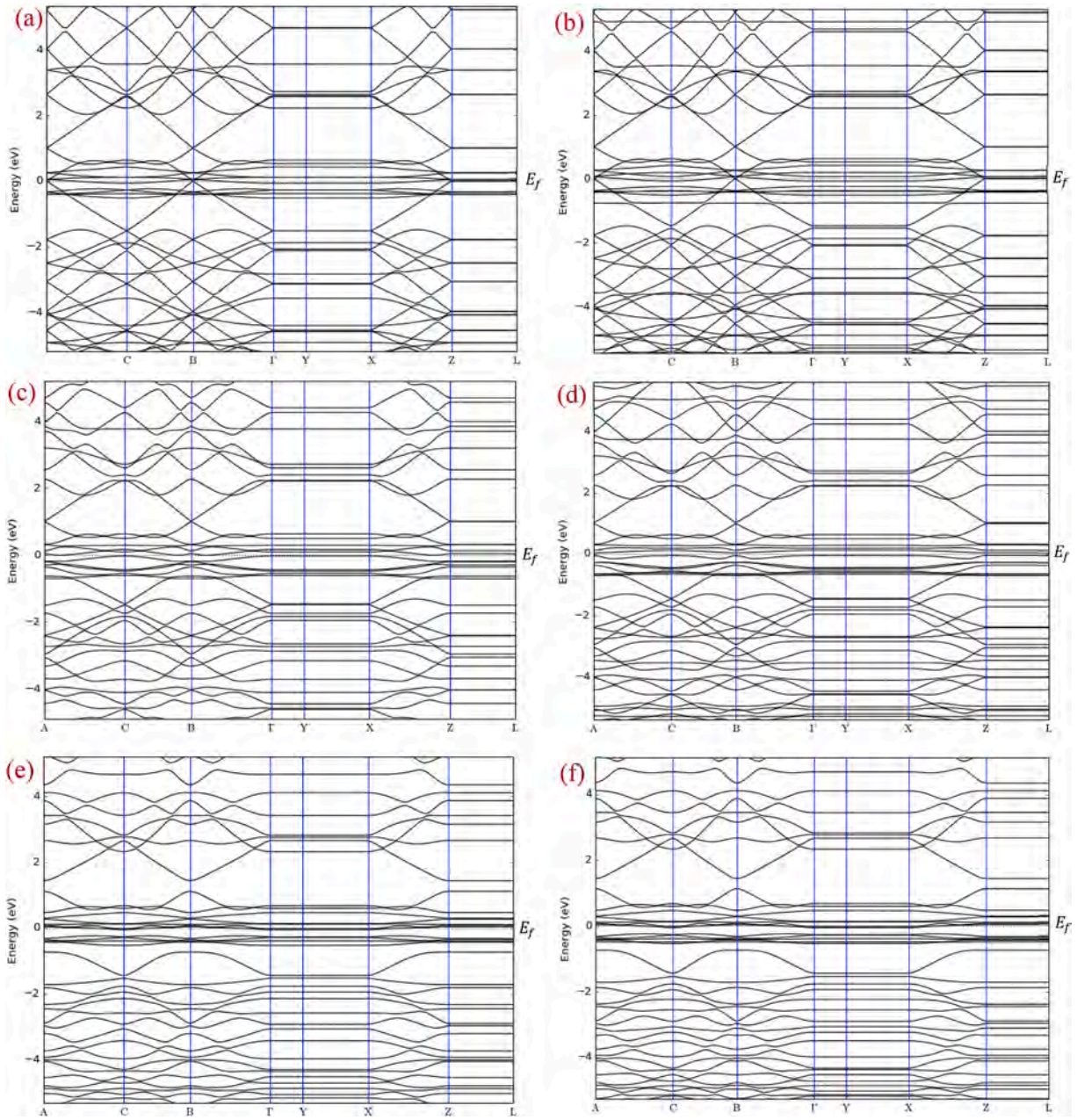

Fig. 8. Band Structure of a) ZGNR, b) ZGNR-H_2S, c) ZGNR-O, d) ZGNR-*O*-H_2S, e) ZGNR-OH, and f) ZGNR–OH–H_2S.

conductance) [54]. Experimental measurements demonstrated that functionalization of graphene surface enable further sensitive and selective performance, as compared with intrinsic graphene, of graphene based sensors [39,55]. For example, reduced graphene oxide was found to be functional for H_2S adsorption at room temperature, and the adsorption is influenced by functional groups of adsorbents [56]. Moreover, functionalizing the surface of graphene oxide with dodecylamine and ethylenediamine had a positive influence on H_2S adsorption as compared with graphene [57].

Experimental measurements as well as many theoretical investigations have been done recently on the adsorption of H_2S gas on pure and modified graphene. For instance, pristine and doped graphene have been used as H_2S sensor [51]. In this study, the adsorption energy in case of H_2S adsorbed on pristine graphene was found to be −0.199 eV, while, upon doping the graphene with phosphorus and silicon the adsorption energy increased to −0.244 and −0.259 eV, respectively [51]. In another study, intrinsic and Fe-doped graphene were used as gas sensors to detect H_2S gas [58]. For the case of intrinsic graphene, the researchers found that the adsorption energy was 0.15 eV. After doping the intrinsic graphene with Fe, the adsorption parameters reflected a significant improvement due to the H_2S binding to Fe-doped graphene through Fe–S bonding [58]. In another study, intrinsic graphene, vacancy

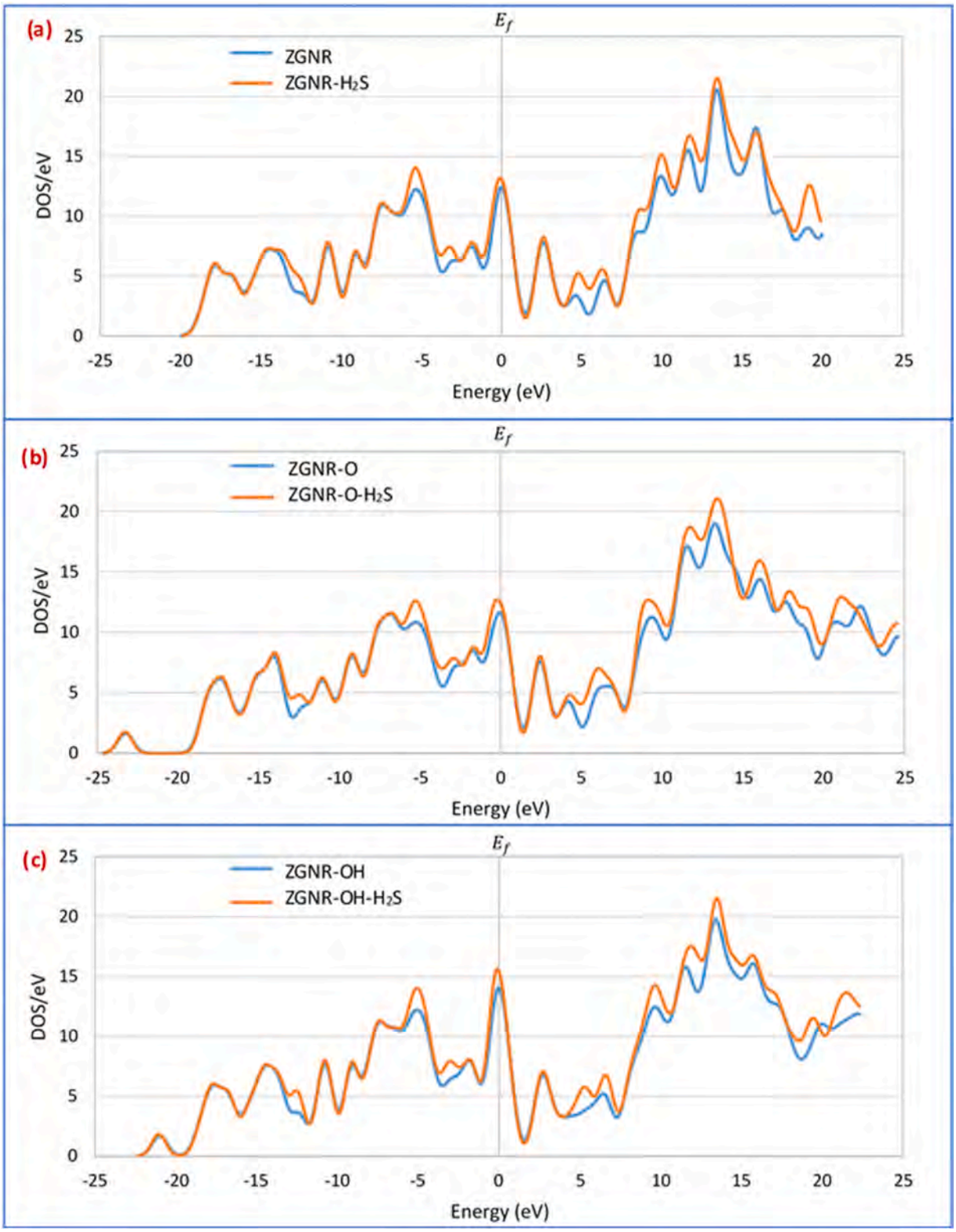

Fig. 9. Density of states of a) ZGNR and ZGNR-H_2S, b) ZGNR-O and ZGNR-*O*-H_2S, and c) ZGNR-OH and ZGNR–OH–H_2S.

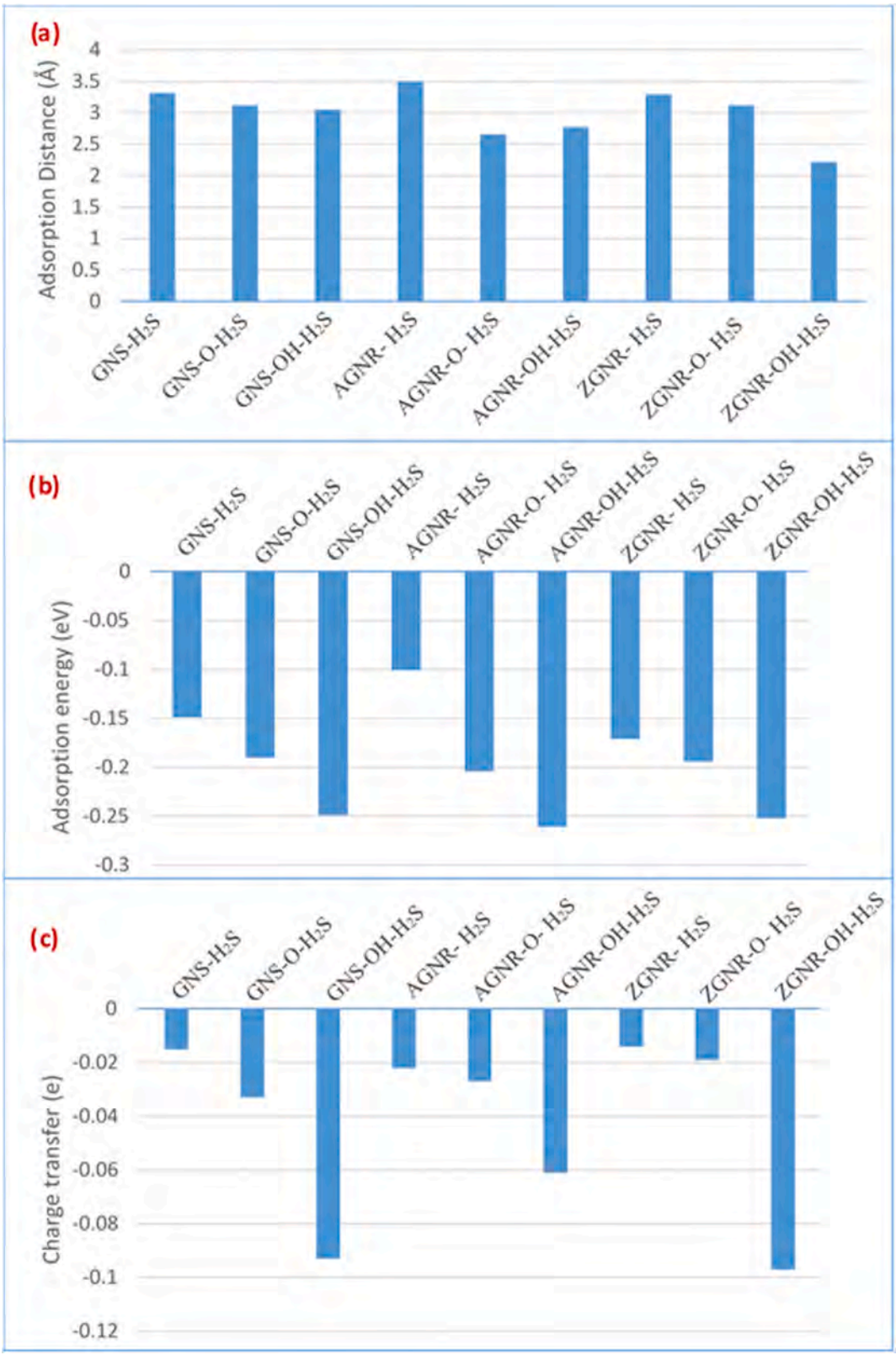

Fig. 10. Comparison between a) adsorption distance, b) adsorption energy, and c) charge transfer between H_2S and GNS, AGNR, and ZGNR systems before and after modification.

defect graphene, Ni-doped graphene, and graphene oxide have been used as a detector for H_2S gas [59]. For the case of intrinsic graphene, the adsorption energy was found between −0.019 and −0.038 eV based on H_2S orientation. These values were remarkably enhanced upon modifying graphene with Ni, vacancy, and –OH group [59]. One more paper in this regard, H_2S adsorption on pristine graphene and graphene decorated with Ni, Pa, and Pt metals have been investigated [48]. It was found that the adsorption energy of H_2S adsorbed on pristine graphene was between 0.122 and 0.201 eV depending on the position and orientation of H_2S [48]. Upon decorating graphene with any of Ni, Pa, and Pt metals, the adsorption capacity demonstrated a remarkable improvement [48]. Moreover, pure ZGNR and AGNR have been also studied as a gas sensor to sense the toxic H_2S gas [60]. The adsorption energies to the gas adsorbed on ZGNR and AGNR were found to be −0.1594 and −0.269 eV, respectively [60]. Whereas, the optimized adsorption distances were found to be 3.36 and 3.50 Å for the cases of ZGNR and AGNR, respectively [60]. The difference between this work and ours is that we further modified the surface of ZGNR and AGNR with epoxy and hydroxyl groups to enhance their adsorption parameters. Interestingly, the adsorption energies, adsorption distances, and charge transfer reflected a remarkable improvement upon the modification.

In addition, many other theoretical investigations have been published recently on the adsorption of the toxic H_2S gas on the surface of graphene based materials and the effect of modifying graphene on the adsorption parameters [61–65]. In the current work, rather than studying one system we compared, in a preliminary study, between the potential of three different graphene based materials to detect the toxic H_2S gas. We then functionalized the surface of these systems to enhance their adsorption capacity toward H_2S adsorption, which have been achieved in accordance with the literatures that have been mentioned above.

4. Conclusion

In conclusion, first principle calculations using the density functional theory (DFT) based on Atomistic ToolKit Virtual NanoLab (ATK-VNL) was used to study H_2S gas sensitivity of graphene nanosheet (GNS), armchair graphene nanoribbons (AGNR), and zigzag graphene nanoribbons (ZGNR) systems. The three systems showed capability toward H_2S gas detection that was quantified using the adsorption energy, binding distance, and charge transfer results. The three systems were modified firstly with epoxy and then with hydroxyl groups to improve their adsorption capacity. The results obtained after the modifications, reflected significant enhancement of the capability of the three systems to adsorb H_2S. Nevertheless, the highest adsorption capacity was observed for the case of ZGNR-OH with adsorption energy of −0.252 eV and −0.097 eV charge transfer. Consequently, hydroxyl modified ZGNR may be considered as a promising candidate for the effective sensing of H_2S gas.

Declaration of competing interest

The authors declare that they have no known competing financial interests or personal relationships that could have appeared to influence the work reported in this paper.

CRediT authorship contribution statement

Ehab Salih: Visualization, Investigation, Writing - original draft. **Ahmad I. Ayesh:** Conceptualization, Methodology, Software, Supervision, Writing - review & editing.

Acknowledgements

Open Access funding provided by the Qatar National Library.

Appendix A. Supplementary data

Supplementary data related to this article can be found at https://doi.org/10.1016/j.spmi.2020.106650.

References

[1] V.A. Ranea, P.L.D. Quiña, N.M. Yalet, General adsorption model for H_2S, H_2Se, H_2Te, NH_3, PH_3, AsH_3 and SbH_3 on the V_2O_5 (0 0 1) surface including the van der Waals interaction, Chem. Phys. Lett. 720 (2019) 58–63.
[2] S. Sriram, V. Nagarajan, R. Chandiramouli, H_2S and NH_3 adsorption characteristics on CoO nanowire molecular device–A first-principles study, Chem. Phys. Lett. 636 (2015) 51–57.
[3] T.W. Lambert, V.M. Goodwin, D. Stefani, L. Strosher, Hydrogen sulfide (H_2S) and sour gas effects on the eye. A historical perspective, Sci. Total Environ. 367 (2006) 1–22.
[4] R. Belley, N. Bernard, M. Côté, F. Paquet, J. Poitras, Hyperbaric oxygen therapy in the management of two cases of hydrogen sulfide toxicity from liquid manure, Can. J. Emerg. Med. 7 (2005) 257–261.
[5] A.I. Ayesh, A.F. Abu-Hani, S.T. Mahmoud, Y. Haik, Selective H_2S sensor based on CuO nanoparticles embedded in organic membranes, Sensor. Actuator. B Chem. 231 (2016) 593–600.
[6] A.I. Ayesh, R.E. Ahmed, M.A. Al-Rashid, R.A. Alarrouqi, B. Saleh, T. Abdulrehman, Y. Haik, L.A. Al-Sulaiti, Selective gas sensors using graphene and CuO nanorods, Sensor Actuator Phys. 283 (2018) 107–112.

[7] M.A. Haija, A.I. Ayesh, S. Ahmed, M.S. Katsiotis, Selective hydrogen gas sensor using $CuFe_2O_4$ nanoparticle based thin film, Appl. Surf. Sci. 369 (2016) 443–447.
[8] A.F. Abu-Hani, Y.E. Greish, S.T. Mahmoud, F. Awwad, A.I. Ayesh, Low-temperature and fast response H_2S gas sensor using semiconducting chitosan film, Sensor. Actuator. B Chem. 253 (2017) 677–684.
[9] R. Srivastava, H. Suman, S. Shrivastava, A. Srivastava, DFT analysis of pristine and functionalized zigzag CNT: a case of H_2S sensing, Chem. Phys. Lett. 731 (2019) 136575.
[10] I.M. El-Sherbiny, E. Salih, Green Synthesis of Metallic Nanoparticles Using Biopolymers and Plant Extracts, Green Metal Nanoparticles: Synthesis, Characterization and Their Applications, 2018, pp. 293–319.
[11] M.S. Dresselhaus, M. Terrones, Carbon-based nanomaterials from a historical perspective, Proc. IEEE 101 (2013) 1522–1535.
[12] S. Iijima, T. Ichihashi, Single-shell carbon nanotubes of 1-nm diameter, Nature 363 (1993) 603.
[13] F.R. Baptista, S. Belhout, S. Giordani, S. Quinn, Recent developments in carbon nanomaterial sensors, Chem. Soc. Rev. 44 (2015) 4433–4453.
[14] S. Bagherzadeh-Nobari, K.H. Istadeh, R. Kalantarinejad, Computational modelling of an amide functionalized single-walled carbon nanotube based H2S gas sensor, Phys. E Low-dimens. Syst. Nanostruct. 115 (2020) 113691.
[15] Z. Yousefian, E. Ghasemy, M. Askarieh, A. Rashidi, Theoretical studies on B, N, P, S, and Si doped fullerenes toward H2S sensing and adsorption, Phys. E Low-dimens. Syst. Nanostruct. 114 (2019) 113626.
[16] M.H. Rashid, A. Koel, T. Rang, M.H. Ziko, Simulations of benzene and hydrogen-sulfide gas detector based on single-walled carbon nanotube over intrinsic 4H-SiC substrate, Micromachines 11 (2020) 453.
[17] M. Oftadeh, M. Gholamian, H.H. Abdallah, Investigation of interaction hydrogen sulfide with (5, 0) and (5, 5) single-wall carbon nanotubes by density functional theory method, Int. Nano Lett. 3 (2013) 7.
[18] O. Faye, U. Eduok, J.A. Szpunar, A.C. Beye, Two-dimensional carbon nitride (C3N) nanosheets as promising materials for H2S and NH3 elimination: a computational approach, Phys. E Low-dimens. Syst. Nanostruct. 117 (2020) 113794.
[19] A.K. Geim, K.S. Novoselov, The rise of graphene, Nat. Mater. 6 (2007) 183–191.
[20] S. Dutta, A.K. Manna, S.K. Pati, Intrinsic half-metallicity in modified graphene nanoribbons, Phys. Rev. Lett. 102 (2009), 096601.
[21] H. Ren, Q.-X. Li, Y. Luo, J. Yang, Graphene nanoribbon as a negative differential resistance device, Appl. Phys. Lett. 94 (2009) 173110.
[22] K.S. Novoselov, A.K. Geim, S.V. Morozov, D. Jiang, Y. Zhang, S.V. Dubonos, I.V. Grigorieva, A.A. Firsov, Electric field effect in atomically thin carbon films, Science 306 (2004) 666–669.
[23] K.S. Novoselov, A.K. Geim, S. Morozov, D. Jiang, M.I. Katsnelson, I. Grigorieva, S. Dubonos, A.A. Firsov, Two-dimensional gas of massless Dirac fermions in graphene, Nature 438 (2005) 197.
[24] S.K. Gupta, G.N. Jaiswal, Study of nitrogen terminated doped zigzag GNR FET exhibiting negative differential resistance, Superlattice. Microst. 86 (2015) 355–362.
[25] A.N.A. Anasthasiya, M. Khaneja, B. Jeyaprakash, Electronic structure calculations of ammonia adsorption on graphene and graphene oxide with epoxide and hydroxyl groups, J. Electron. Mater. 46 (2017) 5642–5656.
[26] Y.-W. Son, M.L. Cohen, S.G. Louie, Half-metallic graphene nanoribbons, Nature 444 (2006) 347.
[27] W. Qiu, P. Nguyen, E. Skafidas, Graphene nanopores: electronic transport properties and design methodology, Phys. Chem. Chem. Phys. 16 (2014) 1451–1459.
[28] A. Wasfi, F. Awwad, A.I. Ayesh, Electronic signature of DNA bases via Z-shaped graphene nanoribbon with a nanopore, Biosens. Bioelectron. X 1 (2019) 100011.
[29] J. Liu, Z. Zhang, X. Deng, Z. Fan, G. Tang, Electronic structures and transport properties of armchair graphene nanoribbons by ordered doping, Org. Electron. 18 (2015) 135–142.
[30] Y. Qiu, X. Zhang, S. Yang, High performance supercapacitors based on highly conductive nitrogen-doped graphene sheets, Phys. Chem. Chem. Phys. 13 (2011) 12554–12558.
[31] H.M. Jeong, J.W. Lee, W.H. Shin, Y.J. Choi, H.J. Shin, J.K. Kang, J.W. Choi, Nitrogen-doped graphene for high-performance ultracapacitors and the importance of nitrogen-doped sites at basal planes, Nano Lett. 11 (2011) 2472–2477.
[32] S. Sharma, A. Verma, A theoretical study of H2S adsorption on graphene doped with B, Al and Ga, Phys. B Condens. Matter 427 (2013) 12–16.
[33] M.D. Ganji, N. Sharifi, M. Ardjmand, M.G. Ahangari, Pt-decorated graphene as superior media for H2S adsorption: a first-principles study, Appl. Surf. Sci. 261 (2012) 697–704.
[34] B. Manna, I. Chakrabarti, P.K. Guha, Platinum nanoparticles decorated graphene oxide based resistive device for enhanced formaldehyde sensing: first-principle study and its experimental correlation, IEEE Trans. Electron. Dev. 66 (2019) 1942–1949.
[35] A. Abbasi, J.J. Sardroodi, TiO_2/graphene oxide heterostructures for gas-sensing: interaction of nitrogen dioxide with the pristine and nitrogen modified nanostructures investigated by DFT, Surf. Rev. Lett. 26 (2019) 1850170.
[36] Y. Gui, Z. Hao, X. Li, C. Tang, L. Xu, Gas sensing of graphene and graphene oxide nanoplatelets to ClO_2 and its decomposed species, Superlattice. Microst. 135 (2019) 106248.
[37] Y. Peng, J. Li, Ammonia adsorption on graphene and graphene oxide: a first-principles study, Front. Environ. Sci. Eng. 7 (2013) 403–411.
[38] N. Osouleddini, S.F. Rastegar, DFT study of the CO_2 and CH_4 assisted adsorption on the surface of graphene, J. Electron. Spectrosc. Relat. Phenom. 232 (2019) 105–110.
[39] A.I. Ayesh, Z. Karam, F. Awwad, M.A. Meetani, Conductometric graphene sensors decorated with nanoclusters for selective detection of Hg2+ traces in water, Sensor. Actuator. B Chem. 221 (2015) 201–206.
[40] E. Salih, A.I. Ayesh, CO, CO_2, and SO_2 detection based on functionalized graphene nanoribbons: first principles study, Phys. E Low-dimens. Syst. Nanostruct. (2020) 114220.
[41] J.P. Perdew, K. Burke, M. Ernzerhof, Generalized gradient approximation made simple, Phys. Rev. Lett. 77 (1996) 3865.
[42] S. Grimme, Semiempirical GGA-type density functional constructed with a long-range dispersion correction, J. Comput. Chem. 27 (2006) 1787–1799.
[43] W. Gao, P. Xiao, G. Henkelman, K.M. Liechti, R. Huang, Interfacial adhesion between graphene and silicon dioxide by density functional theory with van der Waals corrections, J. Phys. Appl. Phys. 47 (2014) 255301.
[44] D. Liu, Y. Gui, C. Ji, C. Tang, Q. Zhou, J. Li, X. Zhang, Adsorption of SF6 decomposition components over Pd (1 1 1): a density functional theory study, Appl. Surf. Sci. 465 (2019) 172–179.
[45] J. Neugebauer, M. Scheffler, Adsorbate-substrate and adsorbate-adsorbate interactions of Na and K adlayers on Al (111), Phys. Rev. B 46 (1992) 16067.
[46] B. Manna, H. Raha, I. Chakrabarti, P.K. Guha, Selective reduction of oxygen functional groups to improve the response characteristics of graphene oxide-based formaldehyde sensor device: a first principle study, IEEE Trans. Electron. Dev. 65 (2018) 5045–5052.
[47] S. Aghaei, M. Monshi, I. Calizo, A theoretical study of gas adsorption on silicene nanoribbons and its application in a highly sensitive molecule sensor, RSC Adv. 6 (2016) 94417–94428.
[48] Z. Bo, X. Guo, X. Wei, H. Yang, J. Yan, K. Cen, Density functional theory calculations of NO_2 and H_2S adsorption on the group 10 transition metal (Ni, Pd and Pt) decorated graphene, Phys. E Low-dimens. Syst. Nanostruct. 109 (2019) 156–163.
[49] R.S. Mulliken, Electronic population analysis on LCAO–MO molecular wave functions. I, J. Chem. Phys. 23 (1955) 1833–1840.
[50] Y. Taluja, B. SanthiBhushan, S. Yadav, A. Srivastava, Defect and functionalized graphene for supercapacitor electrodes, Superlattice. Microst. 98 (2016) 306–315.
[51] V.E.C. Padilla, M.T.R. de la Cruz, Y.E.Á. Alvarado, R.G. Díaz, C.E.R. García, G.H. Cocoletzi, Studies of hydrogen sulfide and ammonia adsorption on P-and Si-doped graphene: density functional theory calculations, J. Mol. Model. 25 (2019) 94.
[52] J. Kroes, M. Akhukov, J. Los, N. Pineau, A. Fasolino, Mechanism and free-energy barrier of the type-57 reconstruction of the zigzag edge of graphene, Phys. Rev. B 83 (2011) 165411.
[53] T. Kawai, Y. Miyamoto, O. Sugino, Y. Koga, Graphitic ribbons without hydrogen-termination: electronic structures and stabilities, Phys. Rev. B 62 (2000) R16349.

[54] S.G. Chatterjee, S. Chatterjee, A.K. Ray, A.K. Chakraborty, Graphene–metal oxide nanohybrids for toxic gas sensor: a review, Sensor. Actuator. B Chem. 221 (2015) 1170–1181.
[55] L. Zhou, F. Shen, X. Tian, D. Wang, T. Zhang, W. Chen, Stable Cu_2O nanocrystals grown on functionalized graphene sheets and room temperature H 2 S gas sensing with ultrahigh sensitivity, Nanoscale 5 (2013) 1564–1569.
[56] M. Khaleghi Abbasabadi, A. Rashidi, J. Safaei-Ghomi, S. Khodabakhshi, R. Rahighi, A new strategy for hydrogen sulfide removal by amido-functionalized reduced graphene oxide as a novel metal-free and highly efficient nanoadsorbent, J. Sulfur Chem. 36 (2015) 660–671.
[57] M.M. Alaie, M. Jahangiri, A. Rashidi, A.H. Asl, N. Izadi, A novel selective H2S sensor using dodecylamine and ethylenediamine functionalized graphene oxide, J. Ind. Eng. Chem. 29 (2015) 97–103.
[58] D. Cortés-Arriagada, N. Villegas-Escobar, D.E. Ortega, Fe-doped graphene nanosheet as an adsorption platform of harmful gas molecules (CO, CO_2, SO_2 and H_2S), and the co-adsorption in O2 environments, Appl. Surf. Sci. 427 (2018) 227–236.
[59] X. Gao, Q. Zhou, J. Wang, L. Xu, W. Zeng, Performance of intrinsic and modified graphene for the adsorption of H2S and CH4: a DFT study, Nanomaterials 10 (2020) 299.
[60] H. Suman, R. Srivastava, S. Shrivastava, A. Srivastava, A. Jacob, C. Malvi, DFT analysis of H2S adsorbed zigzag and armchair graphene nanoribbons, Chem. Phys. Lett. (2020) 137280.
[61] O. Faye, A. Raj, V. Mittal, A.C. Beye, H2S adsorption on graphene in the presence of sulfur: a density functional theory study, Comput. Mater. Sci. 117 (2016) 110–119.
[62] D. Borisova, V. Antonov, A. Proykova, Hydrogen sulfide adsorption on a defective graphene, Int. J. Quant. Chem. 113 (2013) 786–791.
[63] O. Faye, U. Eduok, J. Szpunar, A. Samoura, A. Beye, H2S adsorption and dissociation on NH-decorated graphene: a first principles study, Surf. Sci. 668 (2018) 100–106.
[64] Z. Khodadadi, Evaluation of H2S sensing characteristics of metals–doped graphene and metals-decorated graphene: insights from DFT study, Phys. E Low-dimens. Syst. Nanostruct. 99 (2018) 261–268.
[65] X. Jia, H. Zhang, Z. Zhang, L. An, First-principles investigation of vacancy-defected graphene and Mn-doped graphene towards adsorption of H_2S, Superlattice. Microst. 134 (2019) 106235.